Flexible Mobility Models using Stochastic Differential Equations

Journal:	*IEEE Transactions on Vehicular Technology*
Manuscript ID	VT-2021-01985
Suggested Category:	Regular Paper
Date Submitted by the Author:	09-Jun-2021
Complete List of Authors:	Smith, Peter; Victoria University of Wellington, School of Mathematics, Statistics and Operations Research Singh, Ikram; Victoria University of Wellington, School of Engineering and Computer Science Dmochowski, Pawel; Victoria University of Wellington, School of Engineering and Computer Science Coon, Justin; Oxford University, Engineering Science; Green, Richard; University of Canterbury, Department of Computer Science and Software Engineering
Keywords:	Mobile communication, UAV, Mobility Modeling

Flexible Mobility Models using Stochastic Differential Equations

Peter J. Smith, *Fellow, IEEE*, Ikram Singh, *Student Member, IEEE*, Pawel A. Dmochowski, *Senior Member, IEEE*, Justin P. Coon, *Senior Member, IEEE*, and Richard Green, *Member, IEEE*

***Abstract*—We develop a family of tractable models for UAV mobility. Based on a system of coupled stochastic differential equations, the resulting models exhibit realistic trajectories and flexible covariance structures, making them suitable for both small scale and large scale applications. Closed form solutions for steady state and transient position distributions, as well as position covariance, are derived. These results are subsequently used to obtain distance outage probabilities and pathloss. The analytical results allow us to assess the impact of a variety of system parameters related to device control, navigation and position measurement errors. Finally, using measured UAV flight data, we show an excellent goodness of fit between the proposed model and the data.**

I. Introduction

Autonomous devices are being proposed for applications in an increasing number of environments. These include ground-based robots [1]–[4], unmanned aerial vehicles (UAVs) [5]–[9] and nanobots [10]–[13]. One of the most fundamental questions that can be asked about such systems concerns mobility: How do the devices move? This is critical because location strongly affects connectivity. Secondly, for high precision applications, devices must be able to follow a given path to sufficient accuracy. In this area, the current stochastic mobility models [14]–[19] are overly simplistic, while mechanistic and chaotic models [20]–[23] tend to have no analytical possibilities. For example, simple stochastic models for position, such as Brownian motion (BM) [14] or the Ornstein-Uhlenbeck (OU) [24, p.106] process are physically unrealistic with jagged trajectories and strict constraints on covariance structure. Also, BM has a variance which tends to infinity as time increases [25, p.357]. Similarly, random waypoint models [15] produce simplistic trajectories unless complex variations are adopted. At the other extreme, complex models of device interactions and intelligence [26] lead to interesting mobility behaviour but analytical insights are rare.

This motivates us to design a tractable family of 3D mobility models with more realistic trajectories and flexible covariance structure. The aim is to extend the model-fitting capabilities of the simpler stochastic models while remaining tractable and including a wider range of physical features. For example, we model the effects of environmental perturbations, on-board device control and imperfect navigation. This is achieved through developing a system of coupled stochastic differential equations (SDEs) which model the evolution of position, velocity and navigation error.

There are two broad scenarios in which these models may be useful [27]. In large scale applications, devices are deployed over hundreds of metres or kilometres. Here, the system designer may need mobility models to investigate connectivity issues or communication protocols between devices as the devices traverse a region. In high precision applications, small scale perturbations of the device about a target position are of interest. To model both of these scenarios, we assume a centre or target position around which the devices move. Hence, we will model tethered devices. Extending the work to deterministic flight plans is straightforward.

The two scenarios above also motivate important special cases regarding symmetry in the 3 dimensions. For small scale scenarios, it is reasonable that 3D symmetry is of interest. Over very small distances, the control and perturbation of the device may be the same in each dimension, in the (x, y) horizontal plane and in the z direction (height). Similarly, in large scale scenarios, devices may be widely and equally spread in the (x, y) plane (2D symmetry) with far less variation in height. Hence, we consider all three possibilities: 3D symmetry, 2D symmetry and the general case of full asymmetry.

In particular, we make the following contributions:

- We develop a system of coupled SDEs from which closed form solutions are found for both the steady state and transient distributions of device position.
- The SDEs are also used to derive exact expressions for the covariance structure of position.
- The position distributions are used to derive distance outage probabilities, the probability a device exceeds a given distance from the target. These results also allow us to characterise the path loss between pairs of UAVs.
- We demonstrate the effects of system parameters for control, navigation and error on the location statistics.
- Using measured UAV flight data, we fit the proposed models and show very encouraging agreements between the data and the model.

Notation: Vectors and matrices are denoted by bold lower case and upper case letters respectively. The $(r, s)^{\text{th}}$ element of a matrix $\mathbf{M}_i$ is denoted by M_{irs} or $(\mathbf{M}_i)_{rs}$. Expectation is denoted by $\mathbb{E}\{\cdot\}$, $(\cdot)^T$ represents transpose and $\mathcal{N}(\mu, \sigma^2)$ represents a Gaussian distribution with mean μ and variance σ^2. $\gamma(\cdot, \cdot)$ denotes the lower incomplete gamma function.

P. J. Smith is with the School of Mathematics and Statistics, Victoria University of Wellington, Wellington, New Zealand (e-mail: peter.smith@sms.vuw.ac.nz).

I. Singh and P. A. Dmochowski are with the School of Engineering and Computer Science, Victoria University of Wellington, Wellington, New Zealand (e-mail: {ikram.singh,pawel.dmochowski}@ecs.vuw.ac.nz).

J. P. Coon is with the Department of Engineering Science, University of Oxford, Oxford, U. K. (e-mail: justin.coon@eng.ox.ac.uk).

R. Green is with the Department of Computer Science and Software Engineering, University of Canterbury, Christchurch, New Zealand (e-mail: richard.green@canterbury.ac.nz).

II. Imperfect Navigation

In this section we first motivate and develop the system of coupled SDEs for device position. Using these SDEs we derive the transient distribution of device location (short term distribution where position still depends on the initial location) as well as the steady state position distribution. These are used in later sections to compute path loss statistics and distance outage probabilities. The temporal correlation structure of position is also derived and all results are evaluated for both imperfect and perfect navigation.

A. A System of SDEs for Mobility Modeling

The mobility models presented in this section extend the simple BM and OU processes [24, p.106] to include more realistic device trajectories and imperfect navigation. The simplest SDE for mobility is that which drives BM. For ease of exposition we consider the unidimensional case where X_t is the position of a device at time t in the x-direction. In this scenario, the BM SDE is simply $dX_t = \sigma_1 dB_t$ where $\sigma_1 > 0$ is the diffusion parameter and B_t is standard BM. Note that the subscript, 1, is used here - this denotes the x-dimension and this dimension-dependent notation is needed to separate parameters and processes in 3D. This model gives a position variance, $\mathrm{Var}\{X_t\}$, which is unbounded as $t \to \infty$ [25, p.357] and has a jagged trajectory. The OU process controls BM so that the device has a finite position variance [24, p.107]. This is achieved through a drift parameter, $\alpha_1 > 0$, which controls position by a tendency to revert to the origin. The OU SDE is given by $dX_t = -\alpha_1 X_t + \sigma_1 dB_t$ [24, p.109]. This better models a tethered device but the OU paths remain very jagged.

In order to generate smoother, more realistic trajectories we propose a novel approach where velocity rather than position drives the SDEs. The benefit of this approach is that a smoothing or correlation parameter can be used for velocity as well as a control parameter. The resulting SDE is $dV_{1t} = -\alpha_1 V_{1t} - \beta_1 X_t + \sigma_1 dW_{12t}$ where α_1 models the tendency of the velocity to remain stable and W_{12t} is standard BM. The α parameter correlates the process and smooths out the trajectories. The effect of this new approach can be seen in Fig. 5. The β_1 parameter controls mobility and represents a tendency to adjust the velocity so that the device moves toward the origin. The notation, W_{ijt} is now introduced for BM where i indexes the dimension ($i = 1$ here refers to the x-dimension) and j denotes the process ($j = 2$ refers to velocity). This is clarified in (1).

In practice, the control exerted by the device will depend on the estimated rather than the actual position. Assuming an estimated location, $\hat{X}_t$, which has an evolving error, $\epsilon_{1t} = \hat{X}_t - X_t$, which is a correlated Gaussian process, then the obvious model for ϵ_{1t} is an OU process. Finally, noting that $dX_t = V_{1t}dt$ we have the model equations

$$\left.\begin{aligned} dX_t &= V_{1t}dt \\ dV_{1t} &= -\alpha_1 V_{1t} - \beta_1 \hat{X}_t + \sigma_1 dW_{12t} \\ \epsilon_{1t} &= \hat{X}_t - X_t \\ d\epsilon_{1t} &= -\gamma_1 \epsilon_{1t} + s_1 dW_{13t}, \end{aligned}\right\} \quad (1)$$

where the two standard BM processes, W_{12t} and W_{13t}, are independent. Rewriting (1) in matrix form, the four equations in (1) collapse to

$$d\begin{bmatrix} X_t \\ V_{1t} \\ \epsilon_{1t} \end{bmatrix} = -\begin{bmatrix} 0 & -1 & 0 \\ \beta_1 & \alpha_1 & \beta_1 \\ 0 & 0 & \gamma_1 \end{bmatrix}\begin{bmatrix} X_t \\ V_{1t} \\ \epsilon_{1t} \end{bmatrix} dt + \begin{bmatrix} 0 & 0 & 0 \\ 0 & \sigma_1 & 0 \\ 0 & 0 & s_1 \end{bmatrix} d\begin{bmatrix} W_{11t} \\ W_{12t} \\ W_{13t} \end{bmatrix}. \quad (2)$$

Equation (2) is a multivariate OU process [24, p.109] which can be written in the standard form

$$d\mathbf{S}_{1\mathrm{t}} = -\mathbf{A}_1 \mathbf{S}_{1\mathrm{t}} dt + \mathbf{B}_1 d\mathbf{W}_{1\mathrm{t}}.$$

This discussion was for the position in the x-direction only. Next, we propose to model mobility independently in the three dimensions as in [27]. This is motivated by simplicity and also by measurements of UAV flights where it was found that the correlation between the position in any two dimensions has negligible correlation with the velocity in the third dimension [27]. For example, the (y, z) coordinates of the UAV had little correlation with the velocity in the x-direction (correlation magnitude=0.076) for the flight data in [27].

Hence, the final model is

$$d\mathbf{S}_{\mathrm{it}} = -\mathbf{A}_{\mathrm{i}} \mathbf{S}_{\mathrm{it}} dt + \mathbf{B}_{\mathrm{i}} d\mathbf{W}_{\mathrm{it}}, \ i = 1, 2, 3, \quad (3)$$

where $\mathbf{W}_{1\mathrm{t}}, \mathbf{W}_{2\mathrm{t}}, \mathbf{W}_{3\mathrm{t}}$ are independent, three dimensional BM vectors corresponding to the x, y, z directions respectively. Similarly $\mathbf{S}_{1\mathrm{t}} = [X_t \ V_{1t} \ \epsilon_{1t}]^T$, $\mathbf{S}_{2\mathrm{t}} = [Y_t \ V_{2t} \ \epsilon_{2t}]^T$, $\mathbf{S}_{3\mathrm{t}} = [Z_t \ V_{3t} \ \epsilon_{3t}]^T$ and $\mathbf{A}_{\mathrm{i}}, \mathbf{B}_{\mathrm{i}}$ are parameterized by $\alpha_i, \beta_i, \gamma_i, \sigma_i, s_i$ where $i = 1, 2, 3$ represents the x, y, z directions respectively.

B. SDE Solutions

1) Steady State Distribution: From [28, Sec. 4.5.6], the solution to (3) is Gaussian where the covariance matrix $\mathbf{\Sigma}_i$ of $\mathbf{S}_{\mathrm{it}}$ satisfies $\mathbf{A}_i \mathbf{\Sigma}_i + \mathbf{\Sigma}_i \mathbf{A}_i^T = \mathbf{B}_i \mathbf{B}_i^T$ as $t \to \infty$. Solving this equation by simple linear algebra gives

$$\mathbf{\Sigma}_i = \begin{bmatrix} \frac{\sigma_i^2}{2\alpha_i\beta_i} + \frac{\beta_i s_i^2}{2\alpha_i\gamma_i}\left(\frac{\alpha_i+\gamma_i}{\gamma_{id}}\right) & 0 & \frac{-\beta_i s_i^2}{2\gamma_i\gamma_{id}} \\ 0 & \frac{\sigma_i^2}{2\alpha_i} + \frac{\beta_i^2 s_i^2}{2\alpha_i\gamma_{id}} & \frac{-\beta_i s_i^2}{2\gamma_{id}} \\ \frac{-\beta_i s_i^2}{2\gamma_i\gamma_{id}} & \frac{-\beta_i s_i^2}{2\gamma_{id}} & \frac{s_i^2}{2\gamma_i} \end{bmatrix},$$

where $\gamma_{id} = \gamma_i^2 + \alpha_i\gamma_i + \beta_i$. The resulting steady state distributions for position are $X_t \sim \mathcal{N}(0, \lambda_1), Y_t \sim \mathcal{N}(0, \lambda_2)$ and $Z_t \sim \mathcal{N}(0, \lambda_3)$, where

$$\lambda_i = \frac{\sigma_i^2}{2\alpha_i\beta_i} + \frac{\beta_i s_i^2}{2\alpha_i\gamma_i}\left(\frac{\alpha_i + \gamma_i}{\gamma_i^2 + \alpha_i\gamma_i + \beta_i}\right). \quad (4)$$

2) Transient Distribution: For the transient case, the derivations are more involved and are given in App. A, where it is shown that the transient distributions for position are $X_t \sim \mathcal{N}(0, \lambda_{1t}), Y_t \sim \mathcal{N}(0, \lambda_{2t})$ and $Z_t \sim \mathcal{N}(0, \lambda_{3t})$ where

$$\lambda_{it} = \sum_{r=1}^{3}\sum_{s=1}^{3} V_{i1r} V_{i1s} C_{irs}\left[\frac{1 - e^{-(J_{irr}+J_{iss})t}}{J_{irr} + J_{iss}}\right], \quad (5)$$

with

$$\mathbf{J}_i = \begin{bmatrix} \gamma_i & 0 & 0 \\ 0 & \frac{\alpha_i - \sqrt{\alpha_i^2 - 4\beta_i}}{2} & 0 \\ 0 & 0 & \frac{\alpha_i + \sqrt{\alpha_i^2 - 4\beta_i}}{2} \end{bmatrix} \quad (6)$$

$$\mathbf{V}_i = \begin{bmatrix} \frac{-\beta_i}{\gamma_i^2 - \alpha_i\gamma_i + \beta_i} & \frac{-\alpha_i - \sqrt{\alpha_i^2 - 4\beta_i}}{2\beta_i} & \frac{-\alpha_i + \sqrt{\alpha_i^2 - 4\beta_i}}{2\beta_i} \\ \frac{\beta_i\gamma_i}{\gamma_i^2 - \alpha_i\gamma_i + \beta_i} & 1 & 1 \\ 1 & 0 & 0 \end{bmatrix},$$

and $\mathbf{C}_i = \mathbf{V}_i^{-1}\mathbf{B}_i\mathbf{B}_i^T(\mathbf{V}_i^{-1})^T$.

3) Correlations: In App. B, it is shown that the correlation expressions for X_t, Y_t, Z_t are given by,

$$\rho_i(\tau) = \frac{1}{\lambda_i}\sum_{r=1}^{3}\sum_{s=1}^{3} V_{i1r}(\mathbf{V}_i^{-1})_{rs}\Sigma_{is1}e^{-\tau J_{irr}}, \quad (7)$$

where τ is the time delay and $\mathbf{\Sigma}_i$, $\mathbf{V}_i$ and $\mathbf{J}_i$ are given in Sec. II-B2. Using the established notation, $\rho_1(\tau) = \mathbb{E}\{X_tX_{t+\tau}\}/\mathbb{E}\{X_t^2\}$, $\rho_2(\tau) = \mathbb{E}\{Y_tY_{t+\tau}\}/\mathbb{E}\{Y_t^2\}$ and $\rho_3(\tau) = \mathbb{E}\{Z_tZ_{t+\tau}\}/\mathbb{E}\{Z_t^2\}$.

III. Perfect Navigation

A. A System of SDEs for Mobility Modeling

With perfect navigation, there are no errors in the measurement of the UAV's position. This is equivalent to setting $\gamma_1 = s_1 = \epsilon$ in (2) and allowing $\epsilon \to 0$. Using this limit, the system of SDEs in the x-dimension collapses to

$$d\begin{bmatrix} X_t \\ V_{1t} \end{bmatrix} = -\mathbf{A}_1\begin{bmatrix} X_t \\ V_{1t} \end{bmatrix}dt + \mathbf{B}_1 d\mathbf{W}_{1t} \quad (8)$$

with

$$\mathbf{A}_1 = \begin{bmatrix} 0 & -1 \\ \beta_1 & \alpha_1 \end{bmatrix}, \quad \mathbf{B}_1 = \begin{bmatrix} 0 & 0 \\ 0 & \sigma_1 \end{bmatrix},$$

where α_1, β_1 and σ_1 are defined in Sec. II-A and $\mathbf{W}_{1t}$ is now two-dimensional BM. Equivalent SDEs hold in the y and z-directions. Results for the perfect navigation scenario can be obtained from Sec. II by setting $\gamma_i = s_i \to 0$. As this is only an algebraic exercise, derivations are omitted and the results are summarized below.

B. SDE Solutions

1) Steady State Distribution: From (4), setting $\gamma_i = s_i \to 0$ gives the Gaussian steady state positions, $X_t \sim \mathcal{N}(0, \lambda_1), Y_t \sim \mathcal{N}(0, \lambda_2)$ and $Z_t \sim \mathcal{N}(0, \lambda_3)$ where

$$\lambda_i = \frac{\sigma_i^2}{2\alpha_i\beta_i}. \quad (9)$$

Note that this is equivalent to the standard OU process with a reversion parameter of $\alpha_i\beta_i$. However, the parametrization in (8) via two parameters, α_i and β_i, allows the correlation structure in (11) to be more general than given by the simple OU process.

2) Transient distribution: From (5), setting $\gamma_i = s_i \to 0$ gives the Gaussian positions, $X_t \sim \mathcal{N}(0, \lambda_{1t}), Y_t \sim \mathcal{N}(0, \lambda_{2t})$ and $Z_t \sim \mathcal{N}(0, \lambda_{3t})$, where

$$\lambda_{it} = \frac{\sigma_i^2}{r_i^2}\left[\frac{r_i^2}{2\alpha_i\beta_i} + e^{-\alpha_i t}\left(\frac{2}{\alpha_i} - \frac{e^{r_i t}}{\alpha_i - r_i} - \frac{e^{-r_i t}}{\alpha_i + r_i}\right)\right], \quad (10)$$

and $r_i = \sqrt{\alpha_i^2 - 4\beta_i}$.

3) Correlations: From (7), setting $\gamma_i = s_i \to 0$ gives the following correlation expression

$$\rho_i(\tau) = \frac{1}{2r_i}\left[(\alpha_i + r_i)e^{-\frac{\tau(\alpha_i - r_i)}{2}} + (r_i - \alpha_i)e^{-\frac{\tau(\alpha_i + r_i)}{2}}\right]. \quad (11)$$

IV. Distance Outage Probabilities

We define the distance outage probability as the probability of a UAV exceeding a radial threshold, ie., $P_{\text{out}}(R_0) = P(R_t^2 > R_0^2)$ where $R_t^2 = X_t^2 + Y_t^2 + Z_t^2$. Note that the outage probability expressions presented here are for the transient distributions for position. Results for steady state are simply obtained by replacing the transient λ_{it} parameters by their steady state equivalents, λ_i, for $i = 1, 2, 3$. Results depend on the symmetries between the dimensions and the three scenarios are outlined below.

A. 3D Symmetry

If all of the dimensions of a UAV's position are identically distributed (i.e. $\lambda_{1t} = \lambda_{2t} = \lambda_{3t}$) then it is well known that $R_t^2 \sim \lambda_{1t}\chi_3^2$ where χ_3^2 is a chi-square random variable with 3 degrees of freedom. Using the CDF of χ_3^2 the outage probability is,

$$P_{\text{out}}(R_0) = 1 - \frac{2}{\sqrt{\pi}}\gamma\left(\frac{3}{2}, \frac{R_0^2}{2\lambda_{1t}}\right). \quad (12)$$

B. 2D Symmetry

Here, we only have symmetry in two dimensions. For example, if only X_t and Y_t are identically distributed (i.e. $\lambda_{1t} = \lambda_{2t} \neq \lambda_{3t}$), then it is shown in App. C that the outage probability is

$$P_{\text{out}}(R_0) = 1 - \frac{1}{\sqrt{\pi}}\gamma\left(\frac{1}{2}, \frac{R_0^2}{2\lambda_{3t}}\right) + \frac{e^{-\frac{R_0^2}{2\lambda_{1t}}}}{\sqrt{2\pi w}}\gamma\left(\frac{1}{2}, \frac{wR_0^2}{2\lambda_{3t}}\right), \quad (13)$$

where $w = \frac{1}{2} - \frac{\lambda_{3t}}{2\lambda_{1t}}$. Results for other symmetries between X_t and Z_t and between Y_t and Z_t are easily obtained from (13) by a suitable change of parameters.

C. Fully Asymmetric

If all dimensions are different (i.e. $\lambda_{it} \neq \lambda_{jt}\ \forall i, j$) then R_t^2 is a linear combination of central χ^2 random variables. Using [29, Eq. (35)] the outage probability is

$$P_{\text{out}}(R_0) = 1 - \sum_{k=0}^{\infty} e_k \frac{1}{\Gamma(k + 3/2)}\gamma\left(\frac{2k+3}{2}, \frac{R_0^2}{2\eta}\right), \quad (14)$$

with $\eta = 3\left(1/\lambda_{1t} + 1/\lambda_{2t} + 1/\lambda_{3t}\right)^{-1}$. The coefficients, e_r, are given recursively by

$$e_r = \frac{1}{2r}\sum_{s=0}^{r-1} H_{r-s}e_s, \quad e_0 = \frac{\eta^{3/2}}{\sqrt{\lambda_{1t}\lambda_{2t}\lambda_{3t}}},$$

where $H_k = \sum_{i=1}^{3}(1-\eta/\lambda_{it})^k$. The technique used in [29] to derive (14) expands the PDF of R_t as a linear combination of scaled chi-squared PDFs. The scaling parameter, η, is arbitrary and can be chosen for computational convenience. The value chosen here forces the second coefficient, e_1, to be zero. This tends to accelerate the convergence of (14) by concentrating the main approximation term as the e_0 term with lower order corrections beginning at the e_2 term. Numerically, only 10 terms are usually required in (14) for visually indistinguishable CDFs relative to series truncated after several hundred terms.

D. Large Distance Outages

The exact distance outages in (12), (13) and (14) are given in terms of incomplete gamma functions. To gain more insight into their behaviour, we also consider large distance outages as an important special case, i.e., $P_{\text{out}}(R_0)$ for large R_0. This is achieved mainly through the asymptotic result:

$$\gamma(s,x) \sim \Gamma(s) - x^{s-1}e^{-x}, \tag{15}$$

where $\Gamma(\cdot)$ is the gamma function and x is large and positive.

1) 3D Symmetry: Using (15) in (12) gives

$$P_{\text{out}}(R_0) \sim \sqrt{\frac{2}{\pi\lambda_{1t}}}R_0 e^{-\frac{R_0^2}{2\lambda_{1t}}}. \tag{16}$$

2) 2D Symmetry: When $w > 0$, the arguments of both incomplete gamma functions in (13) are positive. Hence, we can use (15) in both cases and taking the dominant resulting term gives

$$P_{\text{out}}(R_0) \sim \sqrt{\frac{1}{2w}}e^{-\frac{R_0^2}{2\lambda_{1t}}}. \tag{17}$$

When $w < 0$, the argument of the first incomplete gamma function in (13) is positive and we can use (15). The second term gives an incomplete gamma function with a large negative argument. To find an asymptotic result here, we first use

$$\gamma\left(\frac{1}{2}, \frac{wR_0^2}{\lambda_{3t}}\right) = 2jR_0\sqrt{\frac{|w|}{\lambda_{3t}}}M\left(\frac{1}{2}, \frac{3}{2}, \frac{|w|R_0^2}{\lambda_{3t}}\right), \tag{18}$$

where $M(\cdot,\cdot,\cdot)$ is the confluent hypergeometric function of the first kind using [30, Eq. (6.5.12)]. Then, we use the asymptotic result

$$M\left(\frac{1}{2}, \frac{3}{2}, \frac{|w|R_0^2}{\lambda_{3t}}\right) \sim \frac{\lambda_{3t}}{2|w|R_0^2}e^{\frac{|w|R_0^2}{\lambda_{3t}}}, \tag{19}$$

given in [30, Eq. (13.1.4)] for large positive values of the third argument. Using (19) in (18) allows an asymptotic result for the second incomplete gamma function in (13). Substituting in both asymptotic expressions and simplifying gives

$$P_{\text{out}}(R_0) \sim \sqrt{\frac{2\lambda_{3t}}{\pi}}\left(1 + \frac{1}{2|w|}\right)\frac{1}{R_0}e^{-\frac{R_0^2}{2\lambda_{3t}}}. \tag{20}$$

3) Fully Asymmetric: Assume without loss of generality that $\lambda_{1t} > \lambda_{2t} > \lambda_{3t}$. Then, R_t^2 is a linear combination of χ_1^2 variables. Tail probabilities for this scenario are given in [31] as

$$P_{\text{out}}(R_0) = P\left(U > \frac{R_0^2}{\lambda_{1t}}\right)\left(1 - \frac{\lambda_{2t}}{\lambda_{1t}}\right)^{-1/2}\left(1 - \frac{\lambda_{3t}}{\lambda_{1t}}\right)^{-1/2}, \tag{21}$$

where U is a χ_1^2 variable. Now, the tail probability, $P(U > R_0^2/\lambda_{1t})$, can be expressed in terms of an incomplete gamma function and using (15) we obtain the final expression

$$P_{\text{out}}(R_0) \sim \sqrt{\frac{2\lambda_{1t}^3}{\pi(\lambda_{1t}-\lambda_{2t})(\lambda_{1t}-\lambda_{3t})}}\frac{1}{R_0}e^{-\frac{R_0^2}{2\lambda_{1t}}}. \tag{22}$$

4) Large Distance Outage Trends: All the outage results are of the form

$$P_{\text{out}}(R_0) \sim CR_0^{D-2}e^{-\frac{R_0^2}{2\lambda_{it}}}, \tag{23}$$

where $C > 0$ is a constant, D is the number of dominant dimensions and i indexes the dominant dimension. The dominant dimension is the one with the largest λ_{it} value as movement in this dimension is the most likely to become large. As an example, for the 2D symmetry case with $\lambda_{1t} = \lambda_{2t} > \lambda_{3t}$, we have 2 dominant dimensions, labeled dimension 1. Hence, $D = 2$, $i = 1$ and we see that (23) agrees with (17). This simple structure is driven by the simple asymptotic form in (15) which controls the tail probabilities of individual χ^2 variables.

The overall effect is that the exponential term dominates, so that the variance of the dominant direction is critical. The second and lesser effect is the power term in R_0 which inflates large outages as the degree of symmetry is increased.

V. Link Gain Analysis

A key part of any assessment of the communication performance between UAVs or between UAVs and the target is the strength of the link. Here, we characterise these link gains assuming the classical path loss and shadowing model. Hence, the link gain between two devices at time t, distance d_t is given by $P_t = ALd_t^{-\gamma_P}$, where A is the received power at a distance of 1m in the absence of shadowing, γ_P is the path loss exponent and $L = 10^{X/10}$ is log-normal shadowing with $X \sim \mathcal{N}(0, \sigma_{\text{sf}}^2)$ and σ_{sf}^2 being the shadow fading variance. For subsequent analysis, it is convenient to convert the link gain formula to exponential form, so that

$$P_t = Ae^{\beta_P X}d_t^{-\gamma_P}, \tag{24}$$

where $\beta_P = \log_e(10)/10$.

For communication between the UAV and the target then d_t in (24) is given by R_t and full distributional results are available for R_t in Secs. II and III. For communication between two independent UAVs following the same mobility process, we note that the separations between UAV 1 located at $(X_t^{(1)}, Y_t^{(1)}, Z_t^{(1)})$ and UAV 2 located at $(X_t^{(2)}, Y_t^{(2)}, Z_t^{(2)})$ are easily characterized as $(X_t^{(1)} - X_t^{(2)}) \sim \mathcal{N}(0, 2\lambda_{1t})$, $(Y_t^{(1)} - Y_t^{(2)}) \sim \mathcal{N}(0, 2\lambda_{2t})$ and $(Z_t^{(1)} - Z_t^{(2)}) \sim \mathcal{N}(0, 2\lambda_{3t})$. Hence, the distance between two UAVs is statistically identical to the distance between a UAV and the target scaled by $\sqrt{2}$. Therefore, we analyse the link gains between UAV and target, noting that results for communication between two UAVs

follow immediately by replacing A by $2^{-\gamma_P/2}A$. Results are derived for the transient case with steady state equivalents obtained by replacing the transient λ_{it} parameters by their steady state equivalents, λ_i, for $i = 1, 2, 3$.

A. Link Gain Distributions

The CDF of the link gain, $F_P(P_0) = P(P_t \leq P_0)$, is given by conditioning on distance, taking the CDF over the Gaussian shadowing variable and then averaging over distance. This leads to the following integral representation,

$$F_P(P_0) = \frac{1}{2}\int_0^\infty \left[1 + \text{erf}\left(\frac{\ln(P_0 x^{\gamma_P}/A)}{\sqrt{2}\beta_P \sigma_{\text{sf}}}\right)\right] f(x)\, dx, \quad (25)$$

where $f(x)$ is the PDF of the separation distance, d_t, evaluated at x. Note that (25) is general and can be applied to all three mobility scenarios in Sec. IV. Further analytical progress appears difficult, but (25) is well-suited to numeric integration as the integrand is smooth, unimodal and rapidly decaying as x increases. In order to evaluate (25), the distance density is required. This is easily obtained by $f(x) = -\frac{dP_{out}(R_0)}{dR_0}\Big|_{R_0=x}$ where $P_{\text{out}}(R_0)$ is given in Sec. IV. For each scenario, the PDFs are obtained by differentiation as follows

1) 3D Symmetry ($\lambda_{1t} = \lambda_{2t} = \lambda_{3t}$):

$$f(x) = \sqrt{\frac{2}{\pi}}\frac{x^2}{\lambda_{1t}^{3/2}} e^{-x^2/2\lambda_{1t}}. \quad (26)$$

2) 2D Symmetry ($\lambda_{1t} = \lambda_{2t} \neq \lambda_{3t}$):

$$f(x) = \frac{R_0}{\lambda_{1t}\sqrt{2\pi w}}\gamma\left(\frac{1}{2}, \frac{wx^2}{\lambda_{3t}}\right) e^{-x^2/2\lambda_{1t}}. \quad (27)$$

3) Fully Asymmetric ($\lambda_{it} \neq \lambda_{jt}\ \forall i, j$):

$$f(x) = \frac{x}{\eta} e^{-x^2/2\eta} \sum_{k=0}^{\infty} \frac{e_k}{\Gamma(k+3/2)}\left(\frac{x^2}{2\eta}\right)^{k+1/2}, \quad (28)$$

where η and the coefficients e_k are given in Sec. IV.

B. Moments of the Link Gain

The moments of P_t are given by

$$\begin{aligned}\mathbb{E}\left\{P_t^n\right\} &= A^n \mathbb{E}\left\{e^{n\beta_P X}\right\}\mathbb{E}\left\{d_t^{-n\gamma_P}\right\} \\ &= A^n e^{(n\beta_P\sigma_{\text{sf}})^2/2}\mathbb{E}\left\{d_t^{-n\gamma_P}\right\},\end{aligned}$$

using the known moment generating function of a Gaussian. The PDF of d_t is derived in Sec. V-A for three scenarios. Close inspection of (26), (27) and (28) shows that the PDFs, $f(x)$, are $\mathcal{O}(x^2)$ for small x. Hence, $\mathbb{E}\left\{d_t^{-n\gamma_P}\right\}$ is undefined whenever $n\gamma_P > 2$. This limitation is due to the SDEs which place no restriction on mobility leading to the possibility that separation distances are very small. This is very similar to the problem of randomly locating users in a cell where an exclusion zone is usually set around a base-station so that link distances cannot become vanishingly small. Hence, we adopt a similar approach and approximate the moments by assuming a minimum distance, d_{min}, and using the conditional PDF of d_t given $d_t \geq d_{\text{min}}$. Taking this approach, the moments can be approximated by

$$\mathbb{E}\left\{P_t^n\right\} \approx \frac{A^n e^{(n\beta_P\sigma_{\text{sf}})^2/2}}{P_{\text{out}}(d_{\text{min}})}\int_{d_{\text{min}}}^\infty x^{-n\gamma_P} f(x)\, dx, \quad (29)$$

where $f(x)$ and $P_{\text{out}}(d_{\text{min}})$ are scenario specific and given in Sec. V and Sec. IV respectively.

Substituting (26), (27) and (28) into (29) allows the moments to be computed. For the case of 3D symmetry, this gives

$$\mathbb{E}\left\{P_t^n\right\} \approx \frac{2C_0}{\sqrt{\pi(2\lambda_{1t})^{n\gamma_P}}}\Gamma\left(3 - \frac{n\gamma_P}{2}, \frac{d_{\text{min}}^2}{2\lambda_{1t}}\right), \quad (30)$$

and in the fully asymmetric case, we have

$$\mathbb{E}\left\{P_t^n\right\} \approx C_0 \sum_{j=0}^{\infty}\frac{(2\eta)^{-n\gamma_P/2} e_j}{\Gamma(j+3/2)}\Gamma\left(\frac{2j+3-n\gamma_P}{2}, \frac{d_{\text{min}}^2}{2\eta}\right), \quad (31)$$

where $C_0 = A^n \exp\left((n\beta_P\sigma_{\text{sf}})^2/2\right)/P_{\text{out}}(d_{\text{min}})$, $\Gamma(\cdot,\cdot)$ is the upper incomplete gamma function and (30)-(31) follow from an application of the integral in [32, Eq. (3.381.9)]. For the case of 2D symmetry, the moments are not straightforward analytically and numerical results are conveniently obtained by substituting (27) into (29).

VI. Model Fitting

In this section, we describe the measurements of a UAV flight which are used in fitting the SDE models and the model fitting procedure. The dataset used is from an indoor UAV flight in the University of Canterbury Drone Lab. The quad-rotor UAV has a custom built air-frame with a pruning arm for agricultural applications and a total weight of 5 kg. The main platform is 900 mm long and the diagonal centre-prop to centre-prop distance is 600 mm. The on-board control mechanism is a Pixhawk flight controller running PX4. The position of the UAV is measured using camera vision techniques giving positional information accurate to 1 mm for close range operation [33]. Since the UAV uses this highly accurate information for navigation, we fit the models of Sec. III which assume perfect navigation. The 3D positional data during hovering is measured relative to the target, so the x, y, z coordinates are errors from the desired location. Velocities in the three directions are also measured. Discrete time measurements of location and velocity in the x-direction are denoted by $X_1, X_2, \ldots, X_N$ and $V_{1,1}, V_{1,2}, \ldots, V_{1,N}$. The Euler discretization [24, p.376] of the SDE for velocity in the x-direction in (3) is given by

$$V_{1,n+1} - V_{1,n} = -\alpha_1 V_{1,n} - \beta_1 X_n + \sigma_1\sqrt{\Delta t} Z_n, \quad (32)$$

where $n = 1, 2, \ldots, N-1$, Δt is the time gap between discrete measurements and Z_n is a sequence of independent and identically distributed $\mathcal{N}(0,1)$ variables. Rearranging (32) gives the autoregressive formulation

$$V_{1,n+1} = (1-\alpha_1)V_{1,n} - \beta_1 X_n + \sigma_1\sqrt{\Delta t} Z_n. \quad (33)$$

Estimation of the parameters, $\alpha_1, \beta_1, \sigma_1$, can now proceed very simply by ordinary least squares recognizing (33) as a form of linear regression. This is the approach taken here. Note that least squares estimation is a reasonable alternative to the more complex maximum likelihood approach [34].

VII. Results

Here, we verify the analysis presented in this paper, explore the effects of system parameters on mobility and fit the SDE models using measured data from a UAV flight. For reasons of space, most of the results presented are for the more general case of imperfect navigation which includes perfect navigation as a special case. The processes in (3) are simulated via the Euler discretization using $\Delta t = 0.01$ and a total of 10^7 time steps. The resulting discrete process is given for velocity in (32) with similar forms for position and navigation error.

Firstly, in Fig. 1, we consider the distance outage probabilities in Sec. IV for the three types of symmetry (3D symmetry, 2D symmetry and full asymmetry) under both steady state and transient scenarios. Note that the probabilities in (12), (13) and (14) are only functions of the three parameters, $\lambda_{1t}, \lambda_{2t}, \lambda_{3t}$ whereas the original SDEs are defined by $\alpha_i, \beta_i, \gamma_i, s_i, \sigma_i$ for $i = 1, 2, 3$. Hence, we can set $\alpha_i = \beta_i = \gamma_i = s_i = 1$ and allow σ_i and time, t, to vary, giving the desired λ_{it} values.

Steady state parameters for Fig. 1: For the case of 3D symmetry the analysis uses (12) with $\lambda_1 = \lambda_2 = \lambda_3 = 2$ given by $\sigma_1 = \sigma_2 = \sigma_3 = 1.8257$. For 2D symmetry, results are computed using (13) with $\lambda_1 = \lambda_2 = 10, \lambda_3 = 1$ given by $\sigma_1 = \sigma_2 = 4.3970, \sigma_3 = 1.1547$. Finally the asymmetric case is computed using (14) with $\lambda_1 = 2, \lambda_2 = 3, \lambda_3 = 7$ given by $\sigma_1 = 1.8257, \sigma_2 = 2.3094, \sigma_3 = 3.6515$. The 2D symmetry scenario has 10 times more variation in the $x-y$ plane than in height in line with the large scale deployment scenario discussed in Sec. I.

Transient case parameters for Fig. 1: the SDE parameter values are kept unchanged as per the steady state SDEs, except the system is now only simulated for a time of $t = 1$ which resulted in the following transient variances for the three dimension scenarios; $\lambda_{1t} = \lambda_{2t} = \lambda_{3t} = 0.4824$ for 3D symmetry, $\lambda_{1t} = \lambda_{2t} = 2.7238, \lambda_{3t} = 0.2023$ for 2D symmetry and $\lambda_{1t} = 0.4824, \lambda_{2t} = 0.7626, \lambda_{3t} = 1.8833$ for full asymmetry.

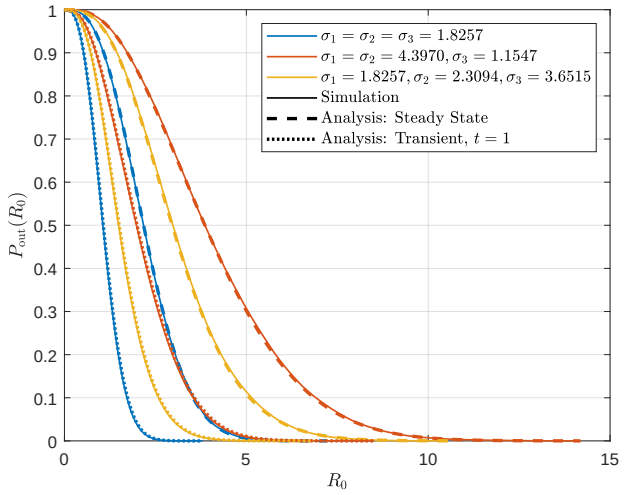

Fig. 1. Distance outage probabilities (steady state and transient).

Fig. 1 demonstrates the following trends, with simulations verifying the analysis in all cases. First, $P_{\text{out}}(R_0)$ decreases as $\sum_{i=1}^{3} \lambda_i$ decreases. In steady state, the highest values are for 2D symmetry ($\sum \lambda_i = 21$) followed by full asymmetry ($\sum \lambda_i = 12$) and the lowest values are for 3D symmetry ($\sum \lambda_i = 6$). This follows the obvious pattern that larger variability in the three dimensions inflates $P_{\text{out}}(R_0)$. Secondly, the transient results are below steady state as the devices had less time to exceed a threshold. Finally, $P_{\text{out}}(R_0)$ values for 3D symmetry in steady state ($\sum \lambda_i = 6$) are very similar to the transient 2D symmetry case ($\sum \lambda_{it} = 5.65$). Hence, the value of $\sum \lambda_i$ or $\sum \lambda_{it}$ may be a useful rule of thumb metric to compare scenarios.

Linking these results back to the individual parameters driving the SDEs we note that λ_i in (4) is an increasing function of σ_i, s_i and a decreasing function of β_i, γ_i, α_i. Hence $P_{\text{out}}(R_0)$ is increased by higher perturbations (larger σ_i, s_i) and decreased by more velocity control (larger β_i), more navigation control (larger γ_i) and more correlated velocity (higher α_i).

Fig. 2 shows asymptotic values of $P_{\text{out}}(R_0)$ using the large distance outage results in (16), (17) and (22). The same steady state parameters are used as in Fig. 1. Not only do the asymptotic results show excellent agreement for large R_0, they are also very accurate for all values of $P_{\text{out}}(R_0)$ below 10^{-1}. Hence, the simple approximation in (23) may have a broad utility.

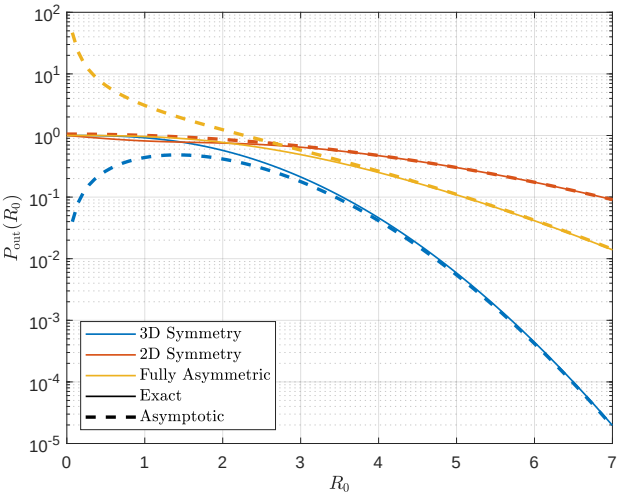

Fig. 2. Large distance outage probabilities.

Next, we consider the correlations in (7) and the cross correlations in (37). In each dimension there are three correlations and three cross correlations as $\mathbf{S}_{it}$ contains three processes. Hence, there are eighteen correlations in total and we necessarily focus on a small subset, giving results for $\rho_1(\tau) = \text{Corr}(X_t, X_{t+\tau})$, using (7), $c_{22}(\tau) = \text{Corr}(V_{1t}, V_{1(t+\tau)})$ and $c_{12}(\tau) = \text{Corr}(X_t, V_{1(t+\tau)})$ using (37). Two parameter sets are used in Fig. 3, $(\alpha_1, \beta_1, \gamma_1, \sigma_1, s_1) = (7, 3, 1, 1, 1)$ and $(\alpha_1, \beta_1, \gamma_1, \sigma_1, s_1) = (1, 3, 7, 1, 1)$. The first set has $\alpha_1^2 - 4\beta_1 = 35 > 0$ giving real diagonal values in $\mathbf{J}_1$ (6) so that correlations in (7) and (37) are given by a sum of three decaying exponentials. This leads to the simple patterns shown in red in Fig. 3. The second set has $\alpha_1^2 - 4\beta_1 = -11 < 0$ so $\mathbf{J}_1$ contains complex entries and the correlations in (7) and (37) include damped sinusoidal variations. In all cases, there is an excellent match between simulations and analysis. Of most interest is the position correlation, $\rho_1(\tau) = \text{Corr}(X_t, X_{t+\tau})$. Here, we

see that the first parameter set yields higher correlations as it has less fluctuation in the navigation error ($\gamma_1 = 1$ rather than $\gamma_1 = 7$) and a higher velocity correlation parameter ($\alpha_1 = 7$ rather than $\alpha_1 = 1$).

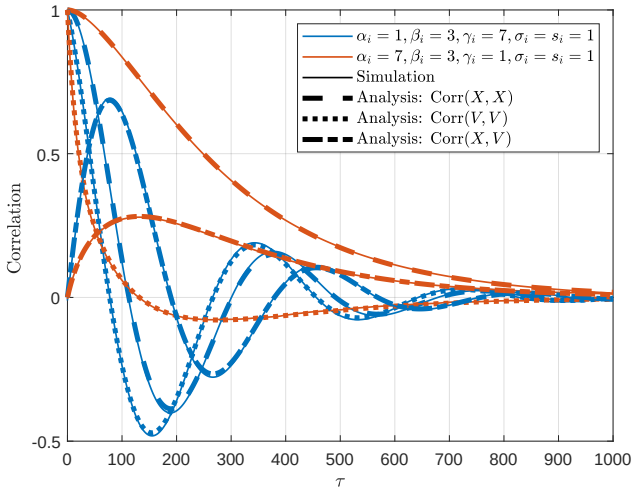

Fig. 3. Positional correlations.

Fig. 4 verifies the path power analyses in Sec. V by plotting the mean link gain against the control parameter $\beta = \beta_1 = \beta_2 = \beta_3$ for $\gamma_P = [2, 3, 4]$, $A = 1, \beta_P = \ln(10)/10, \sigma_{\text{sf}} = 2, d_{\min} = 1, \alpha_i = \beta_i = \gamma_i = s_i = 1$. As

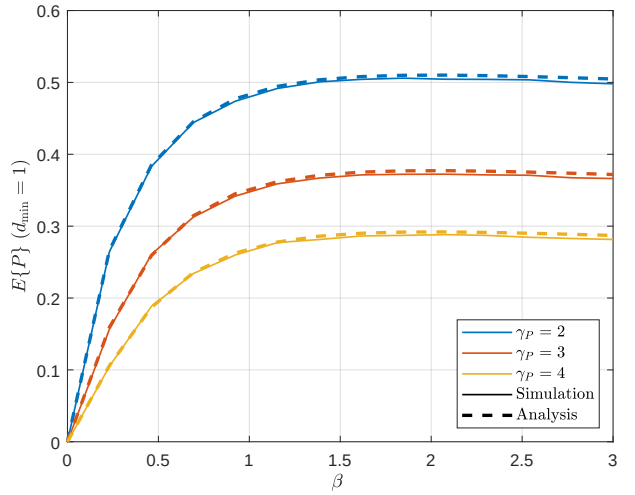

Fig. 4. Mean path power vs. velocity control.

can be seen in Fig. 4, the approximation in the mean path power calculation is quite accurate even for large β_i. Note that large β_i implies tighter control on the mobility so that the UAV does not wander so far and the assumption in (29) that separation $> d_{\min}$ is more restrictive. For small β_i the UAV tends to traverse a larger region in space so the approximation is better in such situations.

Finally, we fit the SDEs in Sec. II-A to actual UAV position data captured by the University of Canterbury UAV Lab, using the methods in Sec. VI.

We demonstrate the resulting fit through sample paths in Fig. 5, position CDFs in Fig. 6 and correlations in Fig. 7. In Fig. 5, we show the measured UAV path in the $x - y$ plane as well as sample paths from an OU process [27] and the proposed SDE (3) using the estimated parameters. It is clear that the OU process is too jagged to model the type of path observed in the data. However, the new SDE model, as designed, smooths out the OU trajectories considerably giving similar features to the measured data. Fig. 6 fits Gaussian CDFs to the measured position in x, y and z and a reasonable agreement is observed. Finally, the more challenging measure of goodness of fit is the temporal correlation in Fig. 7. The analytical correlation agrees with the empirical correlation extremely well all through the main decay from $\rho_1(0) = 1$ to $\rho_1(48) = -0.2$. After that, the empirical correlation appears to lose accuracy due to limited sample size. Overall, these results show an unusually good fit to the model considering the extremely complex realities of UAV control. More data collection is underway to support these conclusions but the model does support a wide range of applications with a simple form, tractable statistics and model-fitting possibilities.

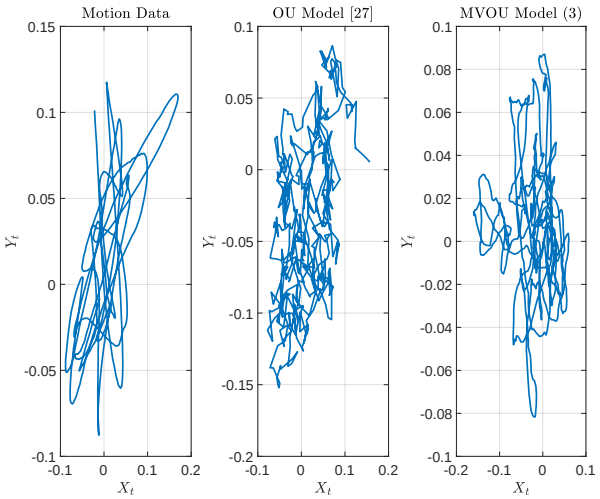

Fig. 5. Sample trajectories.

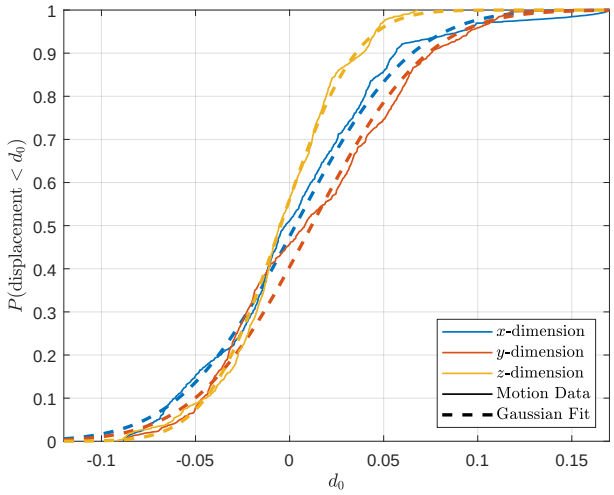

Fig. 6. Empirical CDFs for x, y, z position components.

VIII. Conclusions

We have presented a family of tractable mobility models based on a system of coupled stochastic differential equations,

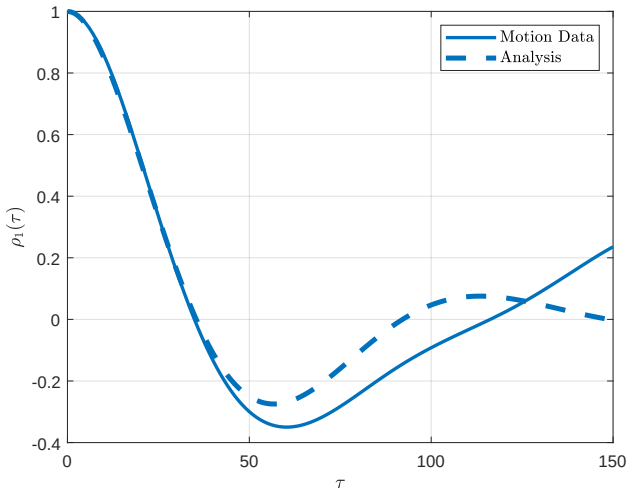

Fig. 7. Temporal position correlation: model and measured UAV data.

suitable for both small scale and large scale UAV applications. We derived closed form solutions for steady state and transient position distributions, position covariance, as well as distance outage probabilities and pathloss. We analysed the impact of a variety of system parameters related to device control, navigation and position measurement errors. Finally, we have confirmed the validity of these models by fitting measured UAV flight data.

Appendix A
Transient Distribution with Imperfect Navigation

Here, we derive the transient distribution for X_t with equivalent results folowing for the y and z-dimensions. Consider the SDE in (3) with $i = 1$ where $\mathbf{S}_{1t} = [X_t, V_{1t}, \epsilon_{1t}]^T$. From [28, Eq. 4.4.45], the covariance matrix related to the transient distribution of $\mathbf{S}_{1t}$ is given by

$$\mathbb{E}\left\{\mathbf{S}_{1t}\mathbf{S}_{1t}^T\right\} = \int_0^t e^{-\mathbf{A}_1(t-t')}\mathbf{B}_1\mathbf{B}_1^T e^{-\mathbf{A}_1^T(t-t')}dt'.$$

Suppose that $\mathbf{A}_1 = \mathbf{V}_1\mathbf{J}_1\mathbf{V}_1^{-1}$ which is the Jordon canonical form of $\mathbf{A}_1$. Then $e^{-\mathbf{A}_1\tau} = \mathbf{V}_1 e^{-\tau\mathbf{J}_1}\mathbf{V}_1^{-1}$, $e^{-\mathbf{A}_1^T\tau} = (\mathbf{V}_1^{-1})^T e^{-\tau\mathbf{J}_1}\mathbf{V}_1^T$ and since the variance of X_t is contained in the $(1,1)^{\text{th}}$ element of $\mathbb{E}\left\{\mathbf{S}_{1t}\mathbf{S}_{1t}^T\right\}$, then

$$\mathbb{E}\left\{X_t^2\right\} = \int_0^t (\mathbf{V}_1)_{1:} e^{(t'-t)\mathbf{J}_1}\mathbf{C}_1 e^{(t'-t)\mathbf{J}_1}(\mathbf{V}_1)_{1:}^T dt', \quad (34)$$

where $(\mathbf{V}_1)_{1:}$ is defined as the first row of $\mathbf{V}_1$ and $\mathbf{C}_1 = \mathbf{V}_1^{-1}\mathbf{B}_1\mathbf{B}_1^T(\mathbf{V}_1^{-1})^T$. Using the Jordon canonical form process [35, pp. 18-21] on $\mathbf{A}_1$ produces the matrices $\mathbf{J}_1$ and $\mathbf{V}_1$ which are given in Sec. II-B2. Expanding (34) gives

$$\begin{aligned}\mathbb{E}\left\{X_t^2\right\} &= \int_0^t \sum_{i=1}^3\sum_{j=1}^3 V_{1i}V_{1j}C_{ij}e^{-(J_{ii}+J_{jj})(t-t')}dt' \\ &= \sum_{i=1}^3\sum_{j=1}^3 V_{1i}V_{1j}C_{ij}\left[\frac{1-e^{-(J_{ii}+J_{jj})t}}{J_{ii}+J_{jj}}\right].\end{aligned}$$

and simple integration leads to (5) as desired.

Appendix B
Position Correlation with Imperfect Navigation

Again, we derive the correlation for X_t, with equivalent results for Y_t and Z_t following similarly. From [28, Eq. 4.4.45], the autocovariance matrix of $\mathbf{S}_{1t}$ is

$$\mathbb{E}\left\{\mathbf{S}_{1(t+\tau)}\mathbf{S}_{1t}^T\right\} = \mathbf{V}_1 e^{-\tau\mathbf{J}_1}\mathbf{V}_1^{-1}\mathbf{\Sigma}_1, \quad (35)$$

where τ is the time delay and $\mathbf{V}_1, \mathbf{J}_1, \mathbf{\Sigma}_1$ are given in Sec. II-B2. Taking the (1,1)-th element of (35), the correlation for X_t is given by

$$\begin{aligned}\rho_1(\tau) &= \frac{\mathbb{E}\left\{X_t X_{t+\tau}\right\}}{(\mathbf{\Sigma}_1)_{11}} = \frac{(\mathbf{V}_1)_{1:}e^{-\tau\mathbf{J}_1}\mathbf{V}_1^{-1}(\mathbf{\Sigma}_1)_{:1}}{\frac{\sigma_1^2}{2\alpha_1\beta_1} + \frac{\beta_1 s_1^2}{2\alpha_1\gamma_1}\left(\frac{\alpha_1+\gamma_1}{\gamma_{1d}}\right)} \quad (36)\\ &= \frac{1}{\frac{\sigma_1^2}{2\alpha_1\beta_1} + \frac{\beta_1 s_1^2}{2\alpha_1\gamma_1}\left(\frac{\alpha_1+\gamma_1}{\gamma_{1d}}\right)}\sum_{r=1}^3\sum_{q=1}^3 V_{11r}(\mathbf{V}_1^{-1})_{rq}\Sigma_{1q1}e^{-\tau J_{1rr}},\end{aligned}$$

where $(\mathbf{\Sigma}_1)_{:1}$ is the first column of $\mathbf{\Sigma}_1$ and $\gamma_{1d} = \gamma_1^2 + \alpha_1\gamma_1 + \beta_1$. Similarly, taking the (i,j)-th element of (35) gives the cross correlation between the i^{th} element of $\mathbf{S}_{1(t+\tau)}$ and the j^{th} element of $\mathbf{S}_{1t}$. This gives

$$c_{ij}(\tau) = \frac{\sum_{r=1}^3\sum_{q=1}^3 V_{1ir}(\mathbf{V}_1^{-1})_{rq}\mathbf{\Sigma}_{1qj}e^{-\tau J_{1rr}}}{\sqrt{\Sigma_{1ii}\Sigma_{1jj}}}. \quad (37)$$

Appendix C
Outage Probability when $\lambda_{1t} = \lambda_{2t} \neq \lambda_{3t}$

When only X_t and Y_t are identically distributed, then the squared radial distance is given by

$$R_t^2 = \lambda_{1t}(X_t^2 + Y_t^2) + \lambda_{3t}Z_t^2 = 2\lambda_{1t}F_{1t} + \lambda_{3t}F_{2t}.$$

where $F_{1t} \sim \text{Exp}(1)$ and $F_{2t} \sim \chi_1^2$. Hence,

$$\begin{aligned}P(R_t^2 \leq R_0^2) &= P(2\lambda_{1t}F_{1t} + \lambda_{3t}F_{2t} \leq R_0^2)\\ &= \mathbb{E}\left\{P\left(2\lambda_{1t}F_{1t} + \lambda_{3t}F_{2t} \leq R_0^2 | F_2\right)\right\}\\ &= \int_0^\infty \frac{e^{-x/2}}{\sqrt{2\pi}\sqrt{x}}P\left(F_{1t} \leq \frac{R_0^2 - \lambda_{3t}x}{2\lambda_{1t}}\right)dx\\ &= \frac{1}{\sqrt{2\pi}}\int_0^{R_0^2/\lambda_{3t}} \frac{e^{-x/2}}{\sqrt{x}}\left(1 - e^{-\frac{R_0^2-\lambda_{3t}x}{2\lambda_{1t}}}\right)dx.\end{aligned}$$

Let $w = \frac{1}{2} - \frac{\lambda_{3t}}{2\lambda_{1t}}$, then the CDF can be reformulated as

$$\begin{aligned}&P(R_t \leq R_0)\\ &= \frac{1}{\sqrt{2\pi}}\left(\int_0^{R_0^2/\lambda_{3t}}\frac{e^{-x/2}}{\sqrt{x}}dx - e^{-\frac{R_0^2}{2\lambda_{1t}}}\int_0^{R_0^2/\lambda_{3t}}\frac{e^{-wx}}{\sqrt{x}}dx\right).\end{aligned}$$

Using [32, Eq. (3.381.1)] the solution for the CDF is

$$P_{\text{out}}(R_0) = \frac{1}{\sqrt{\pi}}\gamma\left(\frac{1}{2}, \frac{R_0^2}{2\lambda_{3t}}\right) - \frac{e^{-\frac{R_0^2}{2\lambda_{1t}}}}{\sqrt{2\pi w}}\gamma\left(\frac{1}{2}, \frac{wR_0^2}{\lambda_{3t}}\right),$$

from which the outage probability in (13) follows.

References

[1] T. Balch and R. Arkin, "Behavior-based formation control for multirobot teams," *IEEE Trans. Robot. Autom.*, vol. 14, no. 6, pp. 926–939, 1998.
[2] Y. Cao *et al.*, "Cooperative mobile robotics: Antecedents and directions," *Autonomous Robots*, vol. 4, no. 1, pp. 7–27, 1997.
[3] Z. Yan *et al.*, "A survey and analysis of multi-robot coordination," *Intern. J. Advanced Robotic Systems*, vol. 10, no. 12, p. 399, 2013.

[4] Y. Rizka *et al.*, "Cooperative heterogeneous multi-robot systems: A survey," *ACM Computing Surveys (CSUR)*, vol. 52, no. 2, pp. 1–31, 2019.
[5] M. Campion *et al.*, "A review and future directions of UAV swarm communication architectures," in *IEEE Intern. Conf. on Electro/Inf. Technol. (EIT)*, 2018, pp. 0903–0908.
[6] ——, "UAV swarm communication and control architectures: A review," *J. Unmanned Vehicle Systems*, vol. 7, no. 2, pp. 93–106, 2018.
[7] E. Kalantari *et al.*, "On the number and 3D placement of drone base stations in wireless cellular networks," in *Proc. of IEEE Veh. Technol. Conf.*, 2016.
[8] R. Palat *et al.*, "Cooperative relaying for ad-hoc ground networks using swarm UAVs," in *Proc. IEEE Military Commun. Conf. (MILCOM)*, Oct. 2005, pp. 1588–1594 Vol. 3.
[9] I. Bor-Yaliniz and H. Yanikomeroglu, "The new frontier in RAN heterogeneity: Multi-tier drone-cells," *IEEE Commun. Mag.*, vol. 54, no. 11, pp. 48–55, Nov. 2016.
[10] S. Dolev *et al.*, "Design of nanorobots for exposing cancer cells," *Nanotechnology*, vol. 30, no. 31, p. 315501, 2019.
[11] V. Loscri and A. Vegni, "An acoustic communication technique of nanorobot swarms for nanomedicine applications," *IEEE Trans. Nanobiosci.*, vol. 14, no. 6, pp. 598–607, 2015.
[12] G. Cerofolini *et al.*, "A surveillance system for early-stage diagnosis of endogenous diseases by swarms of nanobots," *Advanced Science Letters*, vol. 3, no. 4, pp. 345–352, 2010.
[13] Y. Chen *et al.*, "Characterizing nanoscale transient communication," *IEEE Trans. Nanobiosci.*, vol. 15, no. 3, pp. 218–229, Apr. 2016.
[14] T. Camp *et al.*, "A survey of mobility models for ad hoc network research," *Wireless Commun. and Mobile Comput.*, vol. 2, no. 5, pp. 483–502, 2002.
[15] C. Bettstetter *et al.*, "The node distribution of the random waypoint mobility model for wireless ad hoc networks," *IEEE Trans. Mobile Comput.*, vol. 2, no. 3, pp. 257–269, 2003.
[16] P. Sharma *et al.*, "Random 3D mobile UAV networks: Mobility modeling and coverage probability," *IEEE Trans. Wireless Commun.*, vol. 18, no. 5, pp. 2527–2538, May 2019.
[17] P. Nain *et al.*, "Properties of random direction models," in *Proc. Annual Joint Conf. of IEEE Computer and Commun. Societies.*, vol. 3, 2005, pp. 1897–1907.
[18] B. Liang and Z. Haas, "Predictive distance-based mobility management for multidimensional PCS networks," *IEEE/ACM Trans. Netw.*, vol. 11, no. 5, pp. 718–732, Oct. 2003.
[19] M. Banagar *et al.*, *Stochastic Geometry-Based Performance Analysis of Drone Cellular Networks*. John Wiley & Sons, Ltd, 2020, ch. 9, pp. 231–254.
[20] J. Dentler *et al.*, "Collision avoidance effects on the mobility of a UAV swarm using chaotic ant colony with model predictive control," *J. Intelligent and Robotic Systems*, vol. 93, no. 1-2, pp. 227–243, 2019.
[21] M. Rosalie *et al.*, "From random process to chaotic behavior in swarms of UAVs," in *Proc. 6th ACM Symp. on Dev. and Analysis of Intell. Veh. Netw. and Applications*. ACM, 2016, pp. 9–15.
[22] ——, "Chaos-enhanced mobility models for multilevel swarms of UAVs," *Swarm and Evolutionary Computation*, vol. 41, pp. 36–48, 2018.
[23] D. H. Stolfi *et al.*, "A cooperative coevolutionary approach to maximise surveillance coverage of uav swarms," in *2020 IEEE 17th Annual Consumer Communications and Networking Conference (CCNC)*. IEEE, 2020, pp. 1–6.
[24] C. W. Gardiner, *Stochastic Methods: A Handbook for the Natural and Social Sciences*. Springer-Verlag, 2009.
[25] S. M. Ross, *Stochastic processes*, 2nd ed. John Wiley, 1996.
[26] W. Wang *et al.*, "A realistic mobility model with irregular obstacle constraints for mobile ad hoc networks," *Wireless Networks*, vol. 25, no. 2, pp. 487–506, 2019.
[27] P. J. Smith *et al.*, "3D mobility models and analysis for UAVs," in *Proc IEEE International Symposium on Personal, Indoor and Mobile Radio Communications (PIMRC)*, Sep. 2020.
[28] C. W. Gardiner, *Stochastic Methods: A Handbook for the Natural and Social Sciences*. Springer-Verlag, 2009.
[29] N. L. Johnson and S. Kotz, *Continuous Univariate Distributions - Volume 2*. John Wiley and Sons, 1970.
[30] M. Abramowitz and I. A. Stegun, *Handbook of mathematical functions with formulas, graphs, and mathematical tables*. US Government Printing Office, 1964, vol. 55.
[31] R. Beran *et al.*, "Tail probabilities of noncentral quadratic forms," *The Annals of Statistics*, vol. 3, no. 4, pp. 969–974, 1975.
[32] I. S. Gradshteyn and I. M. Ryzhik, *Table of Integrals, Series, and Products*. Elsevier Inc., 2007.
[33] S. Schofield *et al.*, "Calibration for camera-motion capture extrinsics," in *Proc. Intern. Conf. on Image and Vision Comput. New Zealand (IVCNZ)*, Nov. 2018.
[34] J. Bishwal and A. Bose, "Rates of convergence of approximate maximum likelihood estimators in the Ornstein-Uhlenbeck process," *Computers & Mathematics with Applications*, vol. 42, no. 1-2, pp. 23–38, 2001.
[35] S. H. Weintraub, *Jordan Canonical Form: Application to Differential Equations*. Morgan & Claypool Publishers, 2008.